Surface & Coatings Technology xxx (2010) xxx–xxx

Contents lists available at ScienceDirect

Surface & Coatings Technology

journal homepage: www.elsevier.com/locate/surfcoat

Anomalies in Hall-Petch strengthening for nanocrystalline Au–Cu alloys below 10 nm grain size

Alan F. Jankowski *, Luke O. Nyakiti

Texas Tech University, Mechanical Engineering, Box 41021, Lubbock, Texas 79409, USA

ARTICLE INFO

Available online xxxx

Keywords:
Nanocrystalline
Nanohardness
Strain-rate sensitivity

ABSTRACT

The mechanical behavior of an electrodeposited nanocrystalline alloy is assessed with regards to the experimentally measured strain-rate sensitivity. Foils are characterized with grain sizes as small as 3 nm, a nano-scale regime that has previously gone without detailed experimental examination. It is found from micro-scratch measurements that hardness, hence strength, approaches ideal values as the grain size decreases to 7 nm. Below 7 nm, softening in strength and departure from Hall–Petch behavior is related to an increase in the activation volume for deformation as grain size decreases further.

© 2010 Elsevier B.V. All rights reserved.

1. Introduction

The activity of dislocations in macro- to micro- crystalline metals and alloys provides the basis for the Hall–Petch mechanism of material strengthening. In general, a change in strengthening mechanism is believed to occur once the domain size (h_i) decreases below ~10 nm, wherein a transition occurs [1–6] from an intra-granular dislocation-based behavior to an inter-granular boundary motion. A consequence is that the mechanism for Hall–Petch strengthening should be lost with further decrease in grain size (h_g) below ~10 nm. This transition in deformation behavior is dependent on the disorder found [3,6] in the inter-granular boundaries as seen, e.g., in the increasing role of triple junctions. Thus, the nature of the structural disorder in the boundary affects the active deformation mechanism and the concurrent change in strength with a decrease in domain size below 10 nm. Therefore, although a decrease in the activation volume for deformation associated with Hall–Petch strengthening occurs as grain size is reduced from the macro- to micro- to nano-scale, an increase in the activation volume could be associated with the transition to grain boundary mitigated plasticity as the Hall–Petch mechanism begins to breakdown as grain size is reduced below 10 nm.

The scratch-hardness test method is shown as useful to assess [7–9] the mechanical behavior of electrodeposited foils with micro- and nano-crystalline grain structures. Micro-scratch testing gives a measure of hardness, i.e. a yielding of the surface, representative of strength that can be conducted over a wide range of equivalent strain rates where tensile tests are not compatible with a mode of ductile failure. Micro-scratch test results are reported recently [7] that produce strain-rate sensitive measurements comparable with tensile test results.

We now examine the interplay between Hall–Petch type behavior for grain sizes below 10 nm, and those changes related to the activation volume (υ^*) for deformation. It will be shown from the consideration of plastic deformation as a thermally activated process [10–14], that a linear relationship exists between the experimentally determined parameters of "h_i^n/m" and "υ^*". In the first parameter, the domain size can be equated with the grain size (h_g) as raised to an exponent (n) and divided by the strain-rate sensitivity exponent (m). The n represents the power law fit of strength with domain size. For the case of Hall–Petch behavior, n equals negative one-half. The exponent (m) to the power law fit between the strength and strain rate represents the strain-rate sensitivity. The second parameter "υ^*" is the activation volume for deformation that is determined by a linear fit to the logarithmic change in strain rate with its linear change in stress. Since these individual parametric components can be experimentally measured without an a priori assumption to value of the exponent n, an evaluation of Hall–Petch strengthening can be independently made for material behavior as it extends for grain sizes down to a few nanometers. High resolution micrographs of grain structure, and the changes measured in the strain-rate dependent measurement of micro-scratch hardness are now reported for nanocrystalline electrodeposits of gold–copper (Au–Cu).

2. Experimental

The nanocrystalline materials are electrodeposited foils of $Au_{(100-x)}$–$Cu_{(x)}$ ($x<20$ wt.%) that are typically >20 μm thickness. The synthesis method is described [15–18] in full detail elsewhere. The electrodeposition method is based [17] on the control of a pulsed current through a cyanoalkaline solution to produce preselect values of grain size in a fully dense deposit.

* Corresponding author. Texas Tech University, Dept. of Mechanical Engineering, Box 41021, Lubbock, Texas 79416-1021, USA. Tel.: +1 806 742 3563x250; fax: +1 806 742 3540.
E-mail address: alan.jankowski@ttu.edu (A.F. Jankowski).

0257-8972/$ – see front matter © 2010 Elsevier B.V. All rights reserved.
doi:10.1016/j.surfcoat.2010.07.106

In the micro-scratch hardness method, a diamond stylus travels at a velocity (υ) across the specimen surface under a normal incident load (P) producing a scratch with width (ω). It is derived empirically [7] that the strain rate ($\acute{\varepsilon}$) equals the following:

$$\acute{\varepsilon} = \upsilon \cdot \omega^{-1} \quad (1)$$

The micro-scratch hardness (H_s) is computed by dividing the load (P) by the leading area under the indent along the direction of the scratch. A normal incident load (P) of 10 gf, i.e. 98 mN, and scratch indent velocities (υ) of 0.01–1.00 mm sec^{-1} are used during testing. The general expression [8,9] for (H_s) is as follows:

$$H_s = c \cdot P \cdot \omega^{-2} \quad (2)$$

where the constant (c) is an indenter-area term computed from its unique geometric shape. The micro-scratch hardness experiments are conducted using a Center for Tribology, Inc. universal materials tester (UMT-1) equipped with a Rockwell indenter stylus that has a 120° sphero–conical diamond tip and a 12.5 µm radius (r). The width of the micro-scratch profile is measured using a VEECO Dektak (model no. 150) contact profilometer. The measured scratch width (ω), which is usually much greater than its depth, represents the deformation path. The traverse of the scratch profile is made using a diamond stylus with a 0.7 µm tip radius and a tracking load of 98 µN. The specimens for micro-scratch testing are foil cross-sections prepared in an epoxy mount similar to the sample preparation previously used [16] for Vickers microhardness indentation measurements. The specimen surfaces are polished with a final mechanical lapping using half-micron diamond film, and a mild electrochemical etch to remove residual surface damage.

The study of the nanocrystalline foil structure with grain size less than 6 nm is pursued in this investigation using X-ray diffraction (XRD) and transmission electron microscopy (TEM). The crystallite size is quantified by analyzing peak-broadening of the Bragg reflections in Cu k_α X-ray diffraction scans as taken in the $\theta/2\theta$ mode. The crystallite size, i.e. grain size (h_g), is determined [15–17] from the (111) reflections using the standard Debye–Scherrer formulation [19], where the measured peak broadening is corrected for instrument broadening (in addition to the broadening contributions that are attributable to crystallite size). The instrument broadening is determined [7,15] by calibration of the X-ray peak results with measurements from bright-field transmission electron micrographs of specimens with 30–100 nm grain size. The X-ray spectra for nanocrystalline Au–Cu specimens [16] contain all of the fundamental reflections for a face-centered cubic crystal with relative peak intensities that correlate with the standard powder-diffraction file (PDF no. 04-0784) for polycrystalline Au with random texture.

TEM specimens are prepared for examination in plan view as thin foils cut into 3 mm discs using a Gatan 601 Ultrasonic cutter. Specimen thinning then proceeds for electron transparency. First, a dimple grinder reduces the disc thickness to less than 10 µm. Next, ion-polishing proceeds with a Gatan Precision Ion-Polishing System (PIPS) that uses high-purity Argon ion bombardment to further reduce the disc thickness until it is electron transparent. The final polishing is performed by a gradual reduction of the ion beam energy at a glancing angle of incidence angle. The use of low (2.5 keV) milling voltages and a low (4°) milling angle reduces the penetration depth of ions. Thereby, eliminating or reducing [20] any amorphous layer thickness that may be generated as a sample surface artifact, and minimizing any differential thinning effects due to variation in surface topography and mass thickness. The alloy composition is measured from a semi-quantitative analysis of characteristic X-rays generated by an electron beam incident to the specimen surface. The electron-dispersive spectroscopy (EDS) method [3] provides an accuracy of ± 1 wt.% Cu through consideration of atomic number (Z), absorption (A), and fluorescence (F), i.e. a ZAF correction. Again, the grain size (h_g) is determined using the Debye–Scherer X-ray analysis method where instrument broadening of the X-ray peaks are calibrated to an independent measurements of grain size, e.g. as accomplished [15] using TEM bright-field images with a grain size analysis by the lineal intercept method.

3. Results

3.1. Analysis model

The measured mechanical properties are analyzed to determine the strain-rate sensitivity exponent (m) for the nanocrystalline alloy. The strain-rate exponent (m) arises from a power law proportionality of the yield stress (σ) with the strain rate ($\acute{\varepsilon}$), i.e. $\sigma \sim \acute{\varepsilon}^m$, from which the strain-rate exponent (m) is determined by taking the natural logarithm of this proportionality and solving for 'm' as follows:

$$m = [\partial \ln(\sigma)] \cdot [\partial \ln(\acute{\varepsilon})]^{-1}. \quad (3)$$

The linear variation to a logarithmic–logarithmic plot of strain rate ($\acute{\varepsilon}$) with the yield stress (σ^y) yields a slope equivalent to the strain-rate sensitivity exponent (m). For the case of micro-scratch testing [7], the hardness values replace the yield strength values in Eq. (3), i.e. the following:

$$m = [\partial \ln(H_s / H_o)] \cdot [\partial \ln(\acute{\varepsilon})]^{-1} \quad (4)$$

where the scratch hardness (H_s) is computed using Eq. (2), and where the rate of change in H_s can be considered with respect to a baseline value of hardness (H_o) at the lowest strain rate considered for each specimen. A value of $8/\pi$ is used for 'c' in Eq. (2) since the initial stipulation is met that the scratch will have a spherical cross-section since the width (ω) does not exceed the conical tip diameter (2 r) of 25 µm. The imposed criterion of '$\omega < 2$ r' insures that the shape profile of the stylus tip projected onto the specimen during testing is constant, i.e. the constant 'c' is invariant.

The trending of strain rate sensitivity (m) is modeled for the dependence on nanocrystalline metal grain size (h_g). An expression is readily derived [14,21,22] that relates the activation volume (V) for plastic deformation with a characteristic activation length (L) as the following:

$$m = c_1 \cdot (L/V)^{1.5} \cdot \left[\ln\left(L^3/V\right)^{0.5} - c_2\right]^{-1} \quad (5)$$

where the 'c_i' are the constants c_1, c_2, c_3, etc. that are dependent on the shear modulus (G) and Burger's vector (b) for dislocation motion. Eq. (5) can be evaluated further [14,21] using Eq. (1) for the strain-rate sensitivity dependence upon strength. An assumption is made that the Hall–Petch type relationship is applicable, i.e. 'σ' is proportional to '$h_g^{-1/2}$'. A functional relationship between 'h_g' and 'm' then follows as:

$$m = c_3 \cdot [\ln(c_4 \cdot h_i^{0.5}) - c_5]^{-1} \quad (6)$$

where 'V' equals $L \cdot b^2$, and L is proportional to $(h_i)^{0.5}$. A measure of 'h_i' is the grain size 'h_g'. Eq. (6) will be used to fit the variation of 'm' values with h_g for nc Au–Cu and values reported [10] for nc nickel and copper. It is found [7] that for nanocrystalline Au–Cu foils with grain size greater than 7 nm the values of c_3 equals 0.080, c_4 equals 3.0, and c_5 equals 1.65. In comparison, for nanocrystalline Cu [11,23–25] and Ni [10,14,26], the fitted values of c_3 equals 0.036 and 0.018, respectively, whereas both c_4 remains equal to 3.0 and c_5 remains equal to 1.65.

Please cite this article as: A.F. Jankowski, L.O. Nyakiti, Surf. Coat. Technol. (2010), doi:10.1016/j.surfcoat.2010.07.106

ARTICLE IN PRESS

The activation volume (υ^*) that corresponds with the onset of plastic deformation at the yield point, i.e. flow stress, is determined [11,13,14,26] by considering the derivative of the activation enthalpy (ΔH) with respect to stress as follows:

$$\upsilon^* = -[\partial(\Delta H)]\cdot[\partial(\sigma)]^{-1} = \sqrt{3}\cdot k_B\cdot T\cdot[\partial \ln(\dot{\varepsilon})]\cdot[\partial(\sigma)]^{-1} \tag{7}$$

where 'k_B' is the Boltzmann constant and 'T' is the absolute temperature. The linear variation to a semi-logarithmic plot of strain rate ($\dot{\varepsilon}$) with the yield stress (σ^y) yields a slope (multiplied by $k_B\cdot T$) that is equivalent to the activation volume (υ^*). The strength (σ) in Eq. (7) can be approximated by one-third the hardness [14]. In this case the micro-scratch hardness is used, i.e. as σ equals H_s, to quantify the activation volume (υ^*). The strain rate sensitivity exponent (m) and the activation volume (υ^*) are related [11,13,27] according to the relationship as follows:

$$m = \sqrt{3}\cdot k_B\cdot T\cdot(\sigma\cdot\upsilon^*)^{-1} \tag{8}$$

An analysis of these thermal activation parameters seen in Eq. (8) will provide insight to the rate controlling mechanisms in the plastic deformation process. For nanocrystalline metals, any deviation from the Hall–Petch relationship in Eq. (8) is found by considering the inverse square-root dependence of strength on grain size (h_g), and solving for 'υ^*' as follows:

$$\upsilon^*/\sqrt{3} = k_B\cdot T\cdot\left(h_g\right)^{0.5}\cdot(m)^{-1} \tag{9}$$

Therefore, a plot of '$(h_g)^{0.5}\cdot(m)^{-1}$' versus '$\upsilon^*/\sqrt{3}$' should yield a linear relationship where the Hall–Petch relationship is valid, and will deviate from linearity when the Hall–Petch strengthening dependence of dislocation motion in grains is lost when the grain size becomes too small [2,7] to support dislocation-based strengthening.

3.2. Nanocrystalline structure

The nanocrystalline grain size of the Au–Cu electrodeposited foils is quantified [7,15,16,28] using a cross correlation of XRD and high resolution TEM imaging. Structural details of specimens with grain size >6 nm are provided elsewhere [7,15–18,28,29]. A $\theta/2\theta$ XRD scan, in Fig. 1, for a 3 nm grain size 4 wt.% Cu foil reveals the polycrystalline and random orientation nature of the electrodeposited foils. A high resolution TEM image of this specimen in plan view along the z=[011] pole projection in Fig. 2 reveals sub-grain regions on the order of 3 nm in size (within three larger grains) that creates the broad XRD peak seen in Fig. 1. The presence of wide grain boundaries are seen with a high concentration of defects. In comparison [7], the grain boundaries are generally much more narrow with fewer defects in well defined specific crystallographic configurations for grain sizes >5 nm. The boundaries to some of these sub-grains are indicated using solid lines (in Fig. 3) between mosaic regions of coherent scattering as identified using an inverse fast Fourier transform of the region 1 within Fig. 2. Within each grain are domains surrounded by inversion domain boundaries (IDB) as shown in Fig. 4 for a 5 nm grain size Au-5 wt.% Cu sample imaged in plan view. Both dislocations (d) and IDB dislocations are marked in this high resolution TEM image along with some of the grain boundaries (as indicated by dashed lines).

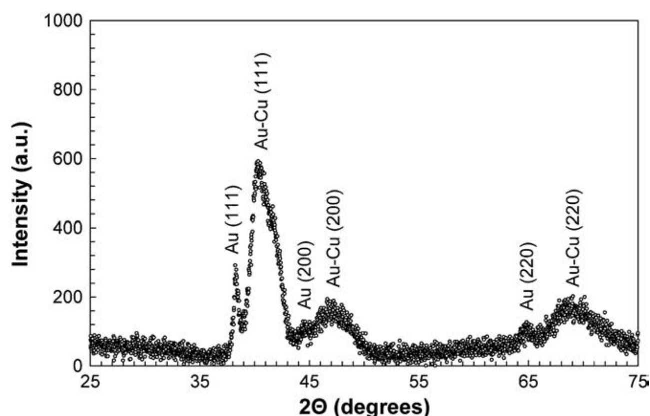

Fig. 1. The X-ray diffraction scan of a 3 nm grain size (h_g) Au-4 wt.% Cu electrodeposited foil as taken using Cu k_α radiation in the $\theta/2\theta$ mode.

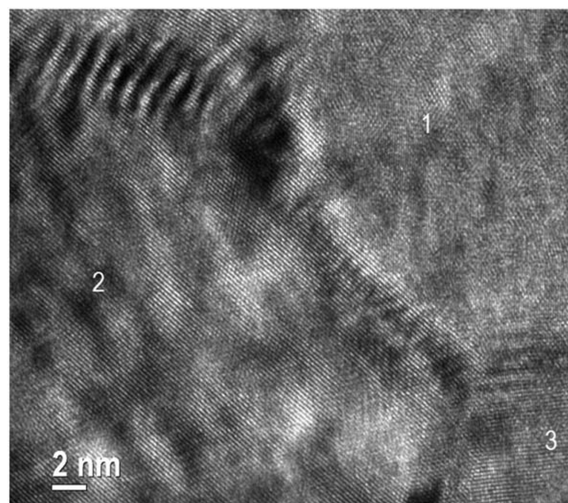

Fig. 2. The high-resolution, transmission electron micrograph of the 3 nm grain size (h_g) Au-4 wt.% Cu sample as imaged in plan view.

3.3. Mechanical properties

The Hall–Petch variation of both micro-indentation hardness [15] and tensile strength [16,29,30] with grain size was investigated in nanocrystalline Au–Cu alloys. New data for the scratch hardness variation with grain size is now presented to account for the effects on strength as manifested through strain rate sensitivity. The dependence of the micro-scratch hardness (H_s) as determined from Eq. (2)

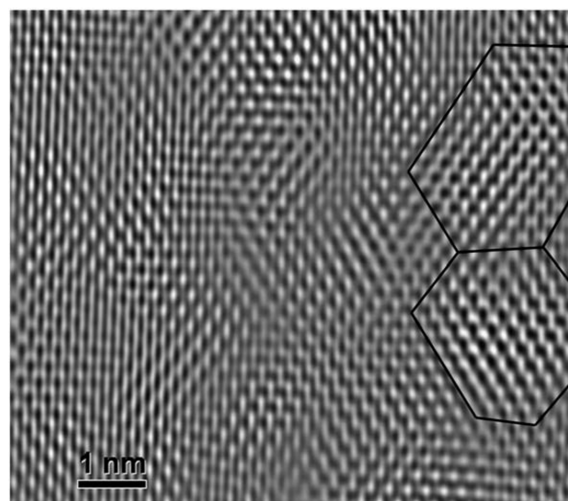

Fig. 3. The inverse fast Fourier transform of region 1 in Fig. 2 reveals a mosaic of sub-grain regions that correspond in an area to the grain size determined from the X-ray diffraction scan of Fig. 1.

Please cite this article as: A.F. Jankowski, L.O. Nyakiti, Surf. Coat. Technol. (2010), doi:10.1016/j.surfcoat.2010.07.106

ARTICLE IN PRESS

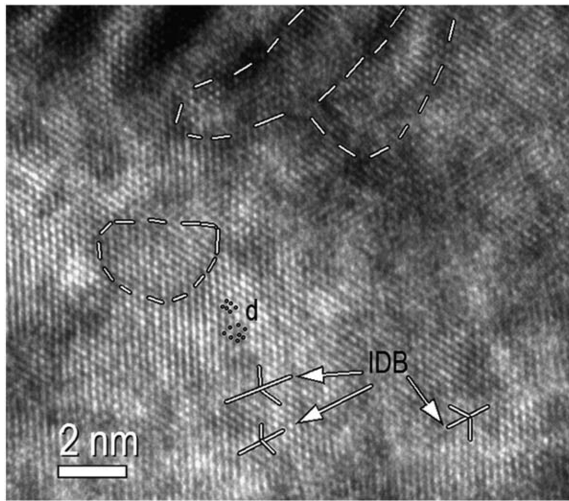

Fig. 4. The dislocations d, inversion domain boundaries (IBD) and some grain boundaries (dashed lines) are noted in the high resolution, transmission electron micrograph of a 5 nm grain size (h_g) Au-5 wt.% Cu sample as imaged in plan view.

on the strain rate ($\dot{\varepsilon}$) as determined from Eq. (1) is used to compute the strain-rate sensitivity exponent (m) as determined from Eq. (4). The new results for several Au–Cu foils with $2.7<h_g<27.3$ nm are now plotted in Fig. 5. Data is considered for all of the linear curves that have a high correlation coefficient, i.e. $R^2>0.9$. The variation of m with h is plotted in Fig. 6 along with $h_g>7$ nm data reported previously for nanocrystalline Au–Cu [7], Cu [10,11,23–25] and Ni [10,14,26]. The curve fits to Eq. (6) are shown as described in the previous section for Analysis model. The variation in m that can occur at a near constant grain size is attributed [7] to the specific crystalline relationship between adjacent grains that, in turn, influence the degrees of freedom in the grain boundary mobility. The Fig. 7 plot shows a linear relationship (where $R^2=0.96$) between υ^* and $(h_g)^{0.5}\cdot(m)^{-1}$ that corresponds to the presence of a Hall–Petch effect according to Eq. (9) for $h_g>5$ nm (open circle data points). In this grain size range, the volume (υ^*) for deformation internal to the grain decreases with the grain size (h_g). In agreement with this trend, the copper data is shown in Fig. 7 inserted as plotted from Eqs. (7–9) computations using experimental data reported [10,11] for m, h_g, and the variation of σ with $\dot{\varepsilon}$ (to determine υ^*). The deviation from the linear fit and the drop in activation volume with decreasing grain size occurs for $h_g<7$ nm (solid circle data points) indicating that the conventional Hall–Petch relationship is no longer valid in this grain size range. There is an overlap region for grain size values between 5 and 7 nm

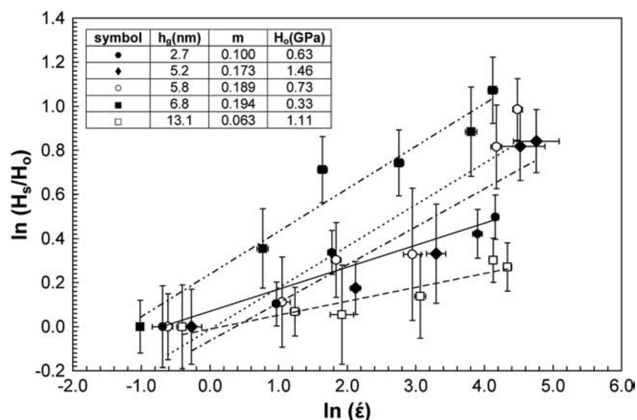

Fig. 5. The strain-rate sensitivity exponent (m) is determined as the slope of the linear variation of ln (H_s/H_o) as a function of ln ($\dot{\varepsilon}$).

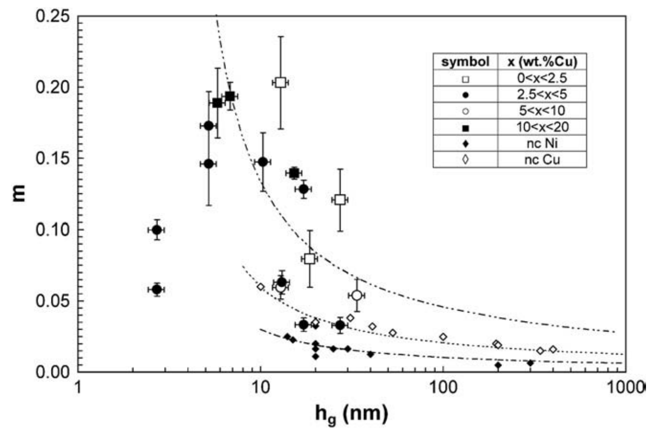

Fig. 6. The strain-rate sensitivity exponent (m) varies with the grain size (h_g).

(open-about-solid circle data points). The increase in υ^* for $h_g<7$ nm in Fig. 7 is consistent with the decrease in m in Fig. 6. The breakdown of the Hall–Petch relationship for strengthening as function of dislocation motion within grains can be modeled using the expression [2] that determines the minimum spacing (h_c) between a pile-up of two dislocations as follows:

$$h_c = G\cdot b\cdot[\pi\cdot(1-\nu)\cdot\sigma]^{-1} \quad (10)$$

where the shear modulus (G), magnitude of the Burger's vector (b), Poisson's ratio (ν), and materials strength (σ) can be computed for the alloy. For a Au-4 wt.% Cu alloy, the G, b, and ν values can be determined using a rule-of-mixtures estimate as 30 GPa, 0.28 nm, and 0.43, respectively. A maximum tensile strength (σ) of 0.60 GPa has been reported [30] for the Au-4 wt.% Cu alloy. Upon substitution of these values in Eq. (10), the minimum spacing (h_c) computed is 7.8 nm — a value that is within range of the $h_g\sim6$ nm determined from the Fig. 7 plot where the breakdown of the Hall–Petch effect occurs.

4. Discussion

The activation volume (υ^*) for deformation is decreased when the grain size decreases from the micro- to nano-scale as seen through the Figs. 6–7 curves as plotted using Eqs. (6) and (9). This trend is found where the conventional Hall–Petch assumption is valid. To support this point, Fig. 7 includes results reported for nano- and micro-crystalline Cu where υ^* decreases with decreasing h_g in agreement with the present nanocrystalline Au–Cu data. However, this trend

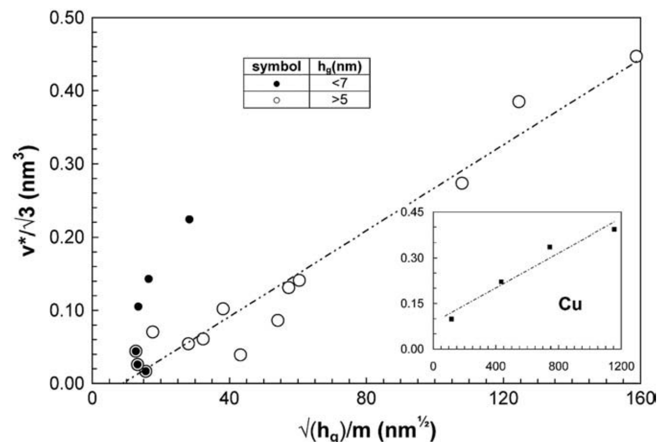

Fig. 7. The activation volume (υ^*) varies linearly as a function of the strain-rate sensitivity exponent (m) and the grain size (h_g) according to the Hall–Petch strength (σ) relationship.

Please cite this article as: A.F. Jankowski, L.O. Nyakiti, Surf. Coat. Technol. (2010), doi:10.1016/j.surfcoat.2010.07.106

ARTICLE IN PRESS

changes when the deformation mode transitions from internal to the grain, to become exterior to the grain. Below a grain size of 5 to 7 nm, the deformation changes as grain boundary sliding and grain rotation become dominant. The activation volume now increases with the inter-granular boundary volume available for deformation wherein conventional dislocation theory is not likely operative and we find evidence for grain boundary mediated plastic deformation.

The transmission electron micrographs of the 3 nm grain size (h_g) Au-4 wt.% Cu sample show regions between the sub-grain boundaries (as associated with size determination from the X-ray diffraction results) that appear to have a non-equilibrium structure, i.e. disorder in the dislocation array. This structural disorder between the grains would be characteristic of: (i) the increase in activation volume (υ^*) for specimens with $h_g < 6$ nm as seen in Fig. 7; (ii) the decrease is sensitivity exponent (m) in Fig. 6; and (iii) the loss of hardness (or strength) which deviates from the Hall–Petch relationship. The micro-scratch hardness measurements are used to quantify the strain-rate exponent (m) by measurement of the variation in scratch hardness (H_s) with strain rate ($\dot{\varepsilon}$) as induced by changing the scratch velocity. An assumption that provides the link between Eqs. (3), (4), and (9) is that a measure for strength (σ) can be determined [31] as a fraction of its hardness. It is important to understand that the ratio between strength and hardness is an approximation that will depend on the specific hardness method in combination with the strain hardening of the material being probed. Since it can be anticipated [32,33] that indentation (H_v) and scratch hardness (H_s) values may differ, we have chosen to use a comparative assessment of the changes in hardness with scratch velocity to determine the sensitivity exponent (m).

5. Conclusion

The use of micro-scratch testing to determine hardness is shown useful to measure the strain-rate sensitivity of strength in nanocrystalline Au–Cu alloys. The loss of Hall–Petch based strengthening is seen in a decrease in strain-rate sensitivity exponent (m) and an increase in activation volume below 5 to 7 nm grain size. This analysis approach overcomes the shortcomings seen in evaluating tensile strength behavior for nanocrystalline alloys that are subject to brittle failure which obscures an analysis of Hall–Petch strengthening.

Acknowledgment

This work is supported through the J.W. Wright Chair Professor Endowment in the Mechanical Engineering Department at Texas Tech University.

References

[1] A.H. Chokshi, A. Rosen, J. Karch, H. Gleiter, Scr. Metall. 23 (1989) 1679.
[2] T.G. Nieh, J.D. Wadsworth, Scr. Metall. Mater. 25 (1991) 955.
[3] M. Ke, S.A. Hackney, W.W. Milligan, E.C. Aifantis, Nanostruct. Mater. 5 (1995) 689.
[4] H. Hahn, K.A. Padmanahan, Nanostruct. Mater. 9 (1997) 603.
[5] C. Schuh, T.G. Nieh, T. Yamasaki, Scr. Mater. 46 (2002) 735.
[6] M.Y. Gutkin, I.A. Ovid'ko, N.V. Skiba, Acta Mater. 52 (2004) 1711.
[7] L.O. Nyakiti, A.F. Jankowski, Metall. Mater. Trans. A 41 (2010) 838.
[8] N. Tayebi, T.F. Conry, A.A. Polycarpou, J. Mater. Res. 18 (2003) 2150.
[9] K.M. Lee, C.-D. Yeo, A.A. Polycarpou, Exp. Mech. 47 (2007) 107.
[10] M. Dao, L. Lu, R.J. Asaro, J.Y.M. De Hosson, E. Ma, Acta Mater. 55 (2007) 4041.
[11] Q. Wei, S. Cheng, K.T. Ramesh, E. Ma, Mater. Sci. Eng. A 381 (2004) 71.
[12] L. Lu, M. Dao, T. Zhu, J. Li, Scr. Mater. 60 (2009) 1062.
[13] J.W. Cahn, F.R.N. Nabarro, Philos. Mag. 81 (2001) 1409.
[14] C.D. Gu, J.S. Lian, Q. Jiang, W.T. Zheng, J. Phys. D Appl. Phys. 40 (2007) 7440.
[15] A.F. Jankowski, C.K. Saw, J.F. Harper, R.F. Vallier, J.L. Ferreira, J.P. Hayes, Thin Solid Films 494 (2006) 268.
[16] A.F. Jankowski, C.K. Saw, J.P. Hayes, Thin Solid Films 515 (2006) 1152.
[17] A.F. Jankowski, Electrochem. Soc. Trans. 1 (12) (2006) 1.
[18] A.F. Jankowski, Defects Diffus. Forum 266 (2007) 13.
[19] B.D. Cullity, Massachusetts 101 (3) (1978) 284.
[20] N.G. Chew, A.G. Cullis, Ultramicroscopy 23 (1987) 175.
[21] J. Lian, C. Gu, Q. Jiang, Z. Jiang, J. Appl. Phys. 99 (2006) 076103.
[22] J. Lian, B. Baudelet, Nanostruct. Mater. 2 (1993) 415.
[23] L. Lu, S.X. Li, K. Lu, Scr. Mater. 45 (2001) 1163.
[24] S. Cheng, E. Ma, Y.M. Wang, L.J. Kecskes, K.M. Youssef, C.C. Koch, U.P. Trociewitz, K. Han, Acta Mater. 53 (2005) 1521.
[25] J. Chen, L. Lu, K. Lu, Scr. Mater. 54 (2006) 1913.
[26] R. Schwaiger, B. Moser, M. Dao, N. Chollacoop, S. Suresh, Acta Mater. 51 (2003) 5159.
[27] G. Taylor, Prog. Mater. Sci. 36 (1992) 29.
[28] L.O. Nyakiti, J. Chaudhuri, A.F. Jankowski, Thin Solid Films 517 (2008) 1182.
[29] Y.M. Wang, A.F. Jankowski, A.V. Hamza, Scr. Mater. 57 (2007) 301.
[30] A.F. Jankowski, NEAT Press, A.S. Khan and B. Farrokh, 2008 pp. 187–189.
[31] J.T. Burwell, C.D. Strang, Mathematical and Physical Sci 212 (1952) 470.
[32] S. Bellemare, M. Dao, S. Suresh, Int. J. Solids Struct. 44 (2007) 1970.
[33] A. Prasad, M. Dao, S. Suresh, Acta Mater. 57 (2009) 511.

Please cite this article as: A.F. Jankowski, L.O. Nyakiti, Surf. Coat. Technol. (2010), doi:10.1016/j.surfcoat.2010.07.106